Journal of Power Sources 186 (2009) 551–556

Contents lists available at ScienceDirect

Journal of Power Sources

journal homepage: www.elsevier.com/locate/jpowsour

Boron and nitrogen co-doped porous carbon and its enhanced properties as supercapacitor

Hongliang Guo, Qiuming Gao*

State Key Laboratory of High Performance Ceramics and Superfine Microstructures, Graduate School, Shanghai Institute of Ceramics, Chinese Academy of Sciences, 1295 Dingxi Road, Shanghai 20050, People's Republic of China

ARTICLE INFO

Article history:
Received 17 June 2008
Received in revised form
11 September 2008
Accepted 8 October 2008
Available online 17 October 2008

Keywords:
Porous carbon
Boron and nitrogen co-doped carbons
Supercapacitor

ABSTRACT

Boron and nitrogen co-doped porous carbons (BNCs) were prepared through a facile procedure using citric acid, boric acid and nitrogen as C, B and N precursors, respectively. The BNC samples were characterized by X-ray diffraction (XRD), X-ray photoelectron spectroscopy (XPS), and nitrogen sorption at 77 K. Cyclic voltammetry and galvanostatic charge/discharge experiments were adopted to investigate their electrochemical behaviors. The BNC-9 and BNC-15 samples with high specific surface areas of 894 and 726 $m^2 g^{-1}$ showed the large specific capacitance up to 268 and 173 $F g^{-1}$, respectively, with the current of 0.1 $A g^{-1}$. When the current was set as 1 $A g^{-1}$, the energy densities were 3.8 and 3.0 Wh kg^{-1} and the power densities were 165 and 201 W kg^{-1} for BNC-9 and BNC-15, respectively. Thus, BNC-15 is more suitable to apply in high-power-demanded occasion, while BNC-9 tends to store more energy.

1. Introduction

Electrical double-layer capacitors (EDLCs), based on charge stored and released along the double layer which forms at the electrode/electrolyte interface, have attracted a great attention in recent years, since they possessed a high power density, quick charge/discharge rate and long cycle-life [1–3]. Carbon materials can be promising candidates for supercapacitor applications because of their chemical stability, low-cost, fine conductivity and kinds of existing forms [2]. Porous carbon materials are interesting due to their high surface area which could be of great importance for high specific capacitance. Various methods were adopted to synthesize porous carbons, including traditional methods [4] such as chemical activation, physical activation, and combination of the physical and chemical activation processes [5–7], carbide-derived carbons [8,9], and newly developed template-synthesized mesoporous/microporous carbons. It is known that the capacitance of carbon materials is closely related to their pore structure and texture. Recently, Gogotsi et al. [8,10] investigated the relationship between the pore sizes of the carbon electrodes and ion sizes of the electrolyte for electrical double-layer capacitors (EDLCs). Their results are in conflict with the traditional attitude toward inaccessibility of small pores to solvated ions and indicate that the micropores largely contribute to the capacitance. Cheng et al. [11] synthesized a kind of porous carbon (HPGC), which combines macroporous cores, mesoporous walls and micropores. The special hierarchical structures lead to fine capacitance retention at a high sweep rate, e.g., the HPGC have a superior frequency response. Besides the influences from the pore structure, the texture of materials can also change the capacitor behaviors. In order to enhance the capacitance, heteroatoms were doped into carbon materials, which not only strengthen the wettability of the interface between electrolyte and electrodes, but also introduce pseudocapacitive effects. Recently, various porous carbon materials, including nitrogen-enriched carbons were massively synthesized. Béguin et al. [12] reported zeolite-templated synthesis of microporous nitrogen-doped carbon, whose specific capacitance was larger than that of nitrogen-free porous carbon with the similar specific surface area and median pore diameters. Zhao et al. [13] obtained nitrogen contained porous carbon by the pyrolysis and carbonization of melamine–formaldehyde resin. Their results showed that the moderate nitrogen content can enhance the surface wettability and reduce the resistance.

Several works have been reported on boron and nitrogen doping carbon materials applied in the fuel cell and Li ion battery [14,15]. And it was reported that the boron doping may improve the specific capacitance per surface area for the multi-walled carbon nanotubes [16]. But their experimental conditions are strict because ultrahigh temperature was necessary for diffusion of the boron atoms into carbon frameworks. Some of the approaches needed moiety-free environment to prevent the boron and carbon precursor from hydrolysis [17]. Besides, our boron dopant quantities are

* Corresponding author. Tel.: +86 21 52412513; fax: +86 21 52413122.
E-mail address: qmgao@mail.sic.ac.cn (Q. Gao).

0378-7753/$ – see front matter © 2008 Elsevier B.V. All rights reserved.
doi:10.1016/j.jpowsour.2008.10.024

higher than that of the reported materials [14,16,17]. In this study, we reported a facile approach to prepare boron and nitrogen co-doped porous carbons through carbonization of the gel containing boron and carbon precursors. The obtained boron and nitrogen enriched carbon materials (denoted as BNC) showed prominent capacitances. These synthetic process avoided toxic carbon precursors such as acetonitrile, formaldehyde, etc. Furthermore, this method has the advantage over the template-synthesized carbons which involving awkward and costly preparation of mesoporous silica or zeolites. The texture and pore structure of the materials can be tuned, whose influences on the capacitive behavior will be discussed in this paper.

2. Experimental

2.1. Preparation of BNC materials

The porous boron and nitrogen co-doped carbon materials were synthesized by pyrolysis and carbonization gels containing boron and carbon precursors under nitrogen flow. The gels were prepared according to the Refs. [18,19]. Typically, 3.85 g of boric acid (AR grade) was dissolved in 50 mL of distilled water at 85 °C. 7.02 g of citric acid (AR grade) was added to the solution, followed by adding 7.0, 9.0, 12.0, and 15.0 g of nickel chloride hexahydrate separately into the solution with stirring. The pH of the solution was adjusted within the range of 2–3 by adding concentrated AR-grade ammonia solution (25 wt.%). Then, the temperature of the solution was set to 110 °C to remove the excess water. After evaporation, the green ropy gels were obtained. The gel was heated at 473 K for 2 h and then 1173 K for 4 h under nitrogen to complete the pyrolysis and carbonization. During the carbonization process, nickel (II) ions were reduced to metal nickel which can be eliminated by dissolving in 2 M hydrochloric acid. The nickel-free materials thus obtained were filtered, washed with deionized water and dried over night, denoted as BNC-7, BNC-9, BNC-12, and BNC-15, where, BNC means the boron and nitrogen co-doped carbon and the number represents the mass of nickel chloride hexahydrate. For comparison, dopant-free carbons (DFC) were prepared following the same procedure except for the addition of boric acid.

2.2. Characterization

Powder X-ray diffraction (XRD) patterns were recorded on a Rigaku D/MAX-2250 V diffractometer with Cu Kα as radiation source (40 kV and 40 mA). The element contents and chemical bonding were investigated by X-ray photoelectron spectroscopy (XPS, Mcrolab 310F with a dual anode X-ray source). Nitrogen adsorption/desorption measurements were carried out at 77 K in Micromeritics ASAP 2020 instrument. The samples were degassed below 1.33 Pa at 90 °C for 1 h and 300 °C for 8 h before the measurements. The specific surface area was calculated based on the Brunauer–Emmett–Teller (BET) method in the relative pressure range of 0.05–0.25. The selected relative pressure range for calculating the surface area was in account with the previous reports which indicate that using a lower relative pressure range, $p/p_0 = 0.01–0.05$, overestimates the surface area while using the higher partial pressure $p/p_0 = 0.1–0.3$ may underestimate the surface area [20,21]. Total pore volume was calculated at a relative pressure $p/p_0 = 0.98$, and Dubinin–Radushikevich (DR) analysis was used to determine the micropore volume in the relative pressure range from 10^{-4} to 10^{-2}. By subtracting the micropore volume from total pore volume, mesopore and macropore volumes were obtained.

Cyclic voltammograms (CV) were tested at different sweep rates with a typical three-electrode configuration in electrolyte of 6 M KOH using CHI 440 (CH Instruments) system. As to the electrode preparation, the porous BNC materials were ground with 10 wt.% polytetrafluoroethylene (PTFE) binder and 10 wt.% acetylene black which helps to increase the conductivity of the electrodes. The mixture was pressed between two pieces of nickel foam (used as a collector) under 30 MPa. Thereafter, the electrode was dried overnight at 100 °C. Ag/AgCl electrode was used as reference electrode, and the counter-electrode was platinum. Galvanostatic charge/discharge behavior was performed under the application of different current densities in the voltage between 0 and 1.0 V with a two-electrode assembled in a button cell system using CT2001A (Land, China) instrument. All the electrochemical tests were performed at room temperature.

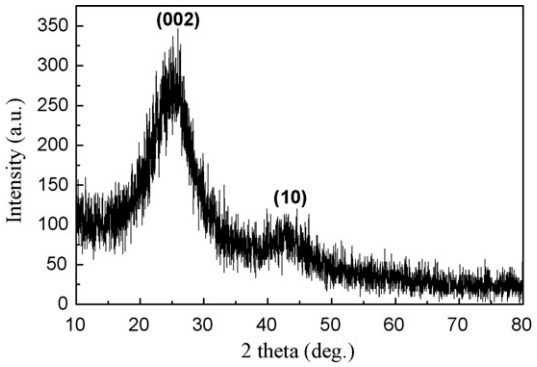

Fig. 1. XRD patterns of the BNC-9.

3. Results and discussion

3.1. Textural and structural properties

XRD patterns of the BNC samples are shown in Fig. 1. Two broad and weak diffraction peaks at 2θ of around 25° and 43° could be observed, which are due to the (0 0 2) and (1 0) lattice planes of turbostratic carbon, respectively. The widened diffraction peaks suggest that no pronounced graphitization occurred under the carbonization temperature of 900 °C. The (0 0 2) peak shifted to a lower angle and the value of d_{002} was 0.356 nm, slightly larger than that of ideal graphite (d_{002} = 0.3354 nm) [22], indicating a low crystallinity of these materials.

The composition and texture of the samples were studied by XPS (Fig. 2). The results show that the carbon materials were doped with

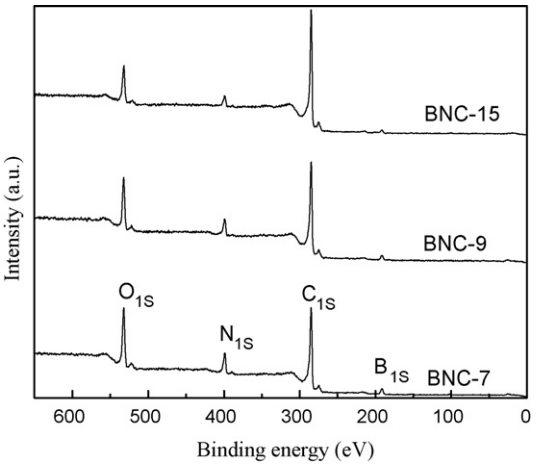

Fig. 2. XPS of the BNC samples.

Table 1
Composition of the BNC samples from XPS.

Samples	at.%			
	B	C	N	O
BNC-7	9.6	63.9	9.2	17.3
BNC-9	8.4	69.8	7.1	14.7
BNC-15	4.8	79.4	4.9	10.9

both boron and nitrogen with the binding energy peak appeared at 191 and 399 eV, respectively. All the samples exhibit almost the same structure due to similar binding energy except for their contents. The C_{1s} peaks were centered at about 285 eV, which could be assigned to the graphite sites in the BNC samples. The oxygen partially comes either from the moisture or carbon dioxide adsorbed on the surface. It is noteworthy that the binding energy of boron and nitrogen in the BNC samples are close to that of boron nitride [23–25]. The nitridization did occur during the pyrolysis and carbonization procedure. However, pure boron nitride phase could not formed because the carbonization temperature was low [26,27] and no related XRD peaks were found. Thus, two adjacent carbon atoms at the periphery of graphite sheets may be substituted by boron and nitrogen atoms simultaneously and the C–B–N bond could exist in this case. Since the electronegativity of O is stronger than that of N, and C is opposite, it could be inferred that C–B–O might be another existing form of B. Increasing the mass of nickel chloride will result in more loss in boron (see Table 1), demonstrating that the reaction between the nickel chloride and boron oxide occurred during the carbonization procedure.

The nitrogen adsorption–desorption isotherms are shown in Fig. 3. All the isotherms are type I mixed with type IV. In low relative pressure range, high adsorption of N_2 occurred, while obvious hystereses were detected, indicating the presence of micropores, mesopores and macropores [28] with the different volume ratios of micropore to mesopore and macropore, respectively. The nitrogen adsorbed below $p/p_0 = 0.02$ may be attributed to the micropore filling. The nitrogen uptake at $p/p_0 = 0.02$–0.2 can be easily observed from the isotherms of BNC-12 and BNC-15, suggesting the presence of super-micropores and small mesopores [29]. The isotherm of BNC-15 also exhibited some limited nitrogen uptake at $p/p_0 > 0.2$, which may be attributed to adsorption into mesopores [30].

The synthetic process of BNC products mainly involved three steps. First, preparation of the gels which were composed of boric acid, citric acid and nickel chloride; then, pyrolysis and carbonization of the gels under inert atmosphere; and at last, etching metal nickel using hydrochloric acid. During the last step in the process, the nickel chloride was reduced to metal by carbon at high temperature and further removed from matrix by using hydrochloric

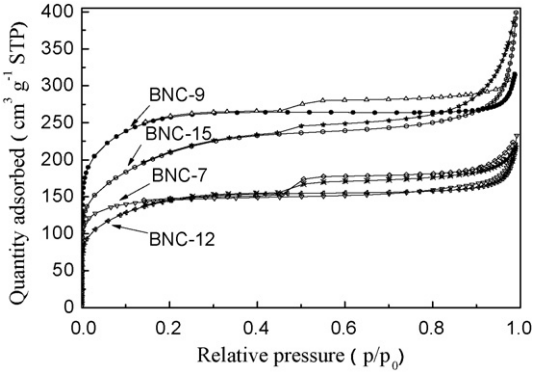

Fig. 3. Adsorption–desorption isotherms of the BNC samples.

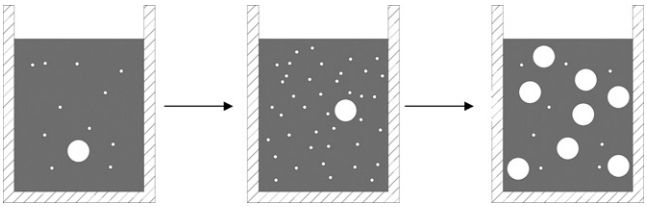

Scheme 1. How the $NiCl_2$ influence the pore structures in the process of preparation. The direction of arrows represents the increase of the $NiCl_2$ gradually; the small white circles are micropores created by nickel complexes and the larger ones are mesopores formed by nickel clusters.

acid, leaving small pores in the products. In addition, hydrochloride from the pyrolysis of nickel chloride might react with boron, generating boron trichloride and escaping away. This process may also create pores, though lose a little of boron. Thus, the quantity of nickel chloride used in the gels may change the pore size distribution (Table 2). It is obvious that the V_{mi} increased from 0.21 cm^3 g^{-1} of BNC-7 to 0.34 cm^3 g^{-1} of BNC-9, while the V_{mea} only increased by 0.1 cm^3 g^{-1}. At meantime, we found that the ratio of micropore volume to total pore volume decreased from 72% to 43%, e.g., large portions of mesopores and macropores formed along with the mass increase of nickel chloride in the gels (BNC-9, 12 and 15), which is due to the formation of different type of clusters polymerized by the nickel complexes at various concentrations. Thus, the BNC materials with regularly changed hierarchical structure can be prepared by carefully changing the mass of nickel chloride as illustrated in Scheme 1. The specific surface area of DFC is 604 m^2 g^{-1}, but the portion of V_{mi} is only 11%. Hence, pyrolysis behavior of the gel without boric acid is totally different from that of BNC precursors.

3.2. Electrochemical tests

CV was used in determination of electrochemical properties of the samples. Fig. 4 shows the CV plots of the BNC samples at a sweep rate of 2 mV s^{-1} with the potential range of −0.9 to −0.1 V vs. Ag/AgCl reference electrode. At this sweep rate all *I–V* curves exhibited near rectangular shapes with slightly distorted, which is characteristic of electrochemical capacitor. Note that wide humps can be clearly observed on the *I–V* plots for BNC-7, 9 and 12, and it is the evident that reversible redox transitions involving proton exchange occurred when the samples were polarized [12]. The deviation from the imaginary rectangular emerged, which is due to the pseudocapacitive effects. An appreciable amount of nitrogen, boron

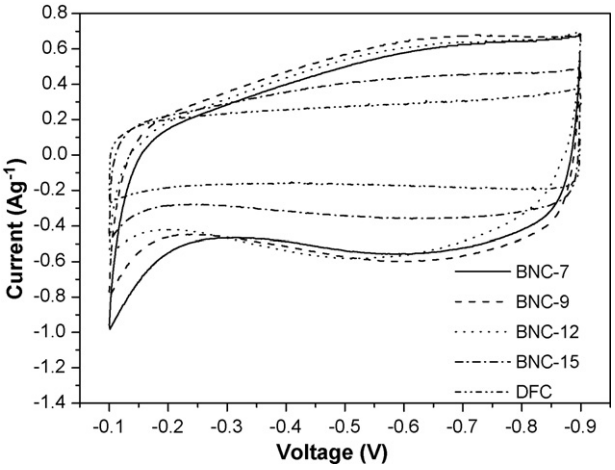

Fig. 4. *I–V* curves of the BNC and DFC samples obtained at 2 mV s^{-1} in 6 M KOH vs. Ag/AgCl.

Table 2
Pore texture properties of BNC and DFC materials.

Samples	S_{BET}[a] ($m^2\,g^{-1}$)	V_t[b] ($cm^3\,g^{-1}$)	V_{mi}[c] ($cm^3\,g^{-1}$)	V_{mea}[d] ($cm^3\,g^{-1}$)	D_{HK}[e] (nm)	D_{BJH} (nm)	V_{mi}/V_t (%)
BNC-7	505	0.33	0.21	0.12	0.49	6.9	64
BNC-9	894	0.47	0.34	0.13	0.59	4.1	72
BNC-12	494	0.33	0.18	0.15	0.64	4.5	55
BNC-15	726	0.60	0.26	0.34	0.62	5.5	43
DFC	604	2.38	0.27	2.11	0.58	15.2	11

[a] BET surface area.
[b] Total pore volume.
[c] Micropore volume determined by using the Dubinin–Radushkevich equation.
[d] Mesopore and macropore volume obtained by subtracting V_{mi} from V_t.
[e] Median micropore diameter calculated by the Horvath–Kawazoe method.

and oxygen incorporated into the carbon matrix can enhance the wettability between the electrolyte and electrode materials, resulting in the pseudocapacitive effect. It was reported that the pyridinic nitrogen at the periphery of the grapheme layers provided electron pairs which may introduce electron donor properties to the layer [31]. According to the electron configuration of boron atom, it may predict that the deficiency of electrons for boron would be more favorable to attract anions in electrolyte compared to that of carbon atom, which may also introduce pseudocapacitance. In order to further prove our viewpoint, dopant-free carbon DFC material was prepared. It apparently shows that although the surface area of sample DFC is comparable to that of the BNC materials, the specific capacitance is only 111 $F\,g^{-1}$ at 2 $mV\,s^{-1}$, less than half of that for BNC-9. So, one might conclude that not only the modification of surface polarity can be achieved by introducing heteroatoms, but also be the pseudocapacitive effect.

Table 3 provides the specific capacitances calculated from the *I–V* plots. In order to reflect the average value of capacitance in the range of sweep voltage, the following equation was used:

$$C = \oint_D \frac{I(U) \times du}{(2 \times \Delta u \times s \times m)} \quad (1)$$

where the integral area is surrounded by *I–V* curve, Δu is the voltage difference, and *s*, *m* are the sweep rate and electrode mass, respectively. BNC-9 has the largest specific capacitance, while the highest capacitance retention value was obtained in BNC-15. It is known that the ions can transport easily in small pores at a low sweep rate. BNC-9 has the most developed micropores with the median pore size of 5.9 Å, which is still larger than that of the dissolved ions ($K^+ \approx H_3O^+ = 3.6–4.2$ Å $> OH^-$) [32]. This means the dissolved ions are allowed to enter the pores, forming the electrical double layers. And the boron and nitrogen dopants modified the polarity of carbon matrixes, which improve the wettability of carbon matrix, providing the possibility that the ions can diffuse into the micropores. Moreover, the dissolved ions have smaller size, which allow a closer approach of the ion center to the electrode surface, leading to improved capacitance [8]. So, it is reasonable that the BNC-9 has the largest capacitance. On the other hand, amount of mesopores were created in BNC-15 due to increasing the mass of nickel chloride. The mesopores provide a short ion-transport pathway [11], which will facilitate forming an electric double layer in a short time. This can explain why BNC-15 has the best capacitance retention among all the samples. The capacitances per surface area (C_{SA}) were calculated. It was found that the values of all the samples are larger than usually reported for the double-layer capacitance (0.1–0.2 $F\,m^{-2}$) [33], which highlight the pseudocapacitive effect of boron and nitrogen co-doping.

Table 3
Specific gravimetric capacitances (C_g) and specific capacitances per surface area (C_{SA}) of all BNC samples as well as DFC.

Samples	C_g ($F\,g^{-1}$)					C_{SA}[a] ($F\,m^{-2}$)
	2 $mV\,s^{-1}$	5 $mV\,s^{-1}$	10 $mV\,s^{-1}$	20 $mV\,s^{-1}$	50 $mV\,s^{-1}$	
BNC-7	229	204	182	149	87	0.45
BNC-9	247	228	206	172	105	0.28
BNC-12	226	200	169	130	73	0.46
BNC-15	170	165	159	151	131	0.23
DFC	111	106	103	99	91	0.18

[a] $C_{SA} = C_g/S_{BET}$, at 2 $mV\,s^{-1}$.

Galvanostatic charge/discharge experiments were performed with various current densities between 0 and 1 V in order to further investigate the performances of representative BNC samples. The specific capacitance of the systems was calculated according to the following equation:

$$C = \frac{2 \times I \times \Delta t}{\Delta V \times m} \quad (2)$$

where *I* is the discharge current, Δt is the time elapsed for the discharge branch from 0.7 to 0.3 V, ΔV is the voltage difference within the time Δt, and *m* is the mass of carbon on an electrode. The factor of 2 comes from the fact that the total capacitance measured from the test cells in the sum of two equivalent single electrode capacitors in series [33–35]. Fig. 5(a) shows the *V–t* plots of BNC-9 and BNC-15 at the constant current of 100 $mA\,g^{-1}$ and Fig. 5(b) is the *V–t* plots of BNC-15 at currents of 0.1, 0.25, 0.5 and 1 $A\,g^{-1}$, respectively.

The charge/discharge curves of both BNC-9 and BNC-15 have near triangular shapes, reflecting their good capacitive performances. The *V–t* plots of BNC-9 and BNC-15 are shown in Fig. 5(a). There was a sharper voltage drop for BNC-9 than that of BNC-15, indicating that the mesopores in BNC-15 sample can improve the ion transfer and may reduce the inner resistance of the electrodes. From the galvanostatic charge/discharge curves at different current densities in Fig. 5(b), we can see that BNC-15 possessed typical triangular shapes with a little galvanostatic discharge decrease caused by the inner resistance throughout the current range of 1–0.1 $A\,g^{-1}$, showing its good capacitive properties. The specific capacitances determined by Eq. (2) (from Table 4) are 268 and 173 $F\,g^{-1}$ with the current of 0.1 $A\,g^{-1}$ for BNC-9 and BNC-15, respectively. The data agree well with those obtained from CV tests. When the applied current was increased from 0.1 to 1 $A\,g^{-1}$, the capacitances remained 59% and 72% for BNC-9 and BNC-15, respectively. And the coincident trend has been found in the CV tests.

Power density and energy density also estimated using the following equations:

$$E = \frac{CV^2}{2} \quad (3)$$

$$P = \frac{E}{t} \quad (4)$$

Table 4
Specific gravimetric capacitance (C_g), energy density (E) and power density (P) data estimated by Eqs. (2)–(4).

Currents ($A\,g^{-1}$)	BNC-9			BNC-15		
	C_g ($F\,g^{-1}$)	E ($Wh\,kg^{-1}$)	P ($W\,kg^{-1}$)	C_g ($F\,g^{-1}$)	E ($Wh\,kg^{-1}$)	P ($W\,kg^{-1}$)
0.1	268	6.7	20	173	4.6	21
0.25	235	5.8	47	160	4.4	52
0.5	216	5.1	91	152	3.9	99
1	158	3.8	165	125	3.0	201

where C, V and t are the specific gravimetric, cell voltage and discharge time, respectively. From Table 3 and Fig. 5(c), we can see that the power density of BNC-15 is larger than that of BNC-9, although BNC-9 possesses the larger energy density at the same constant current. For example, when the current was set as $1\,A\,g^{-1}$, the energy densities and power densities for BNC-9 and BNC-15 were 3.8/3.0 $Wh\,kg^{-1}$ and 165/201 $W\,kg^{-1}$, respectively. Thus, BNC-15 may be more suitable to apply in high-power-demanded occasion, while BCN-9 tends to store more energy.

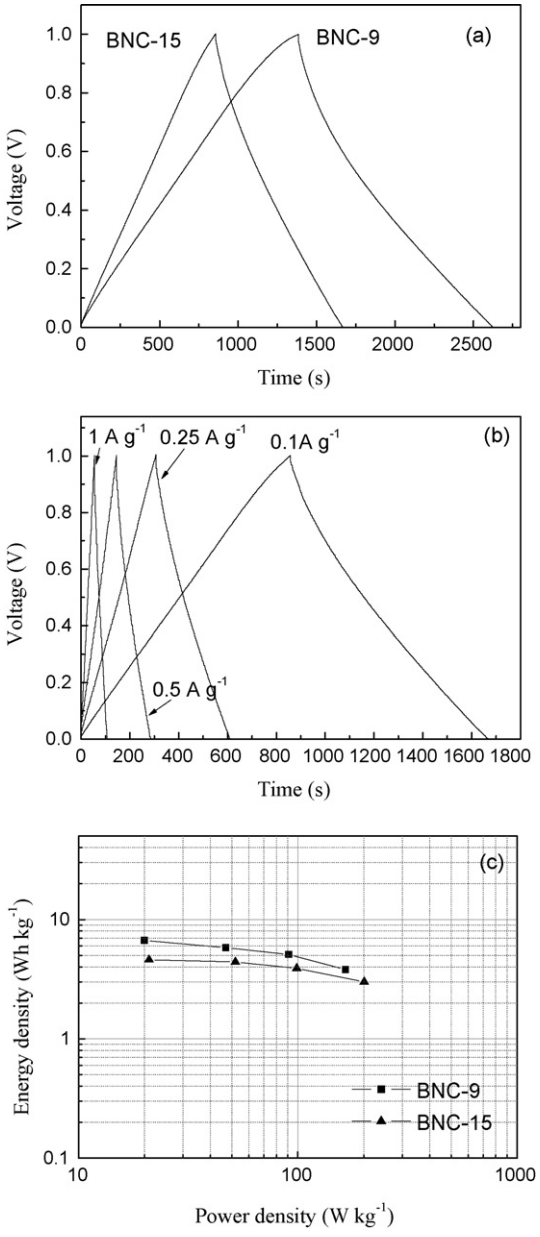

Fig. 5. (a) V–t plots of BNC-9 and BNC-15 with current $100\,mA\,g^{-1}$; (b) V–t plots of BNC-15 with currents of 0.1, 0.25, 0.5, and $1\,A\,g^{-1}$; and (c) Ragone plot for BNC-9 and BNC-15 in KOH electrolyte.

4. Conclusions

Boron and nitrogen co-doped porous carbon materials were synthesized through a facile procedure including nickel-contained gel preparation, and carbonization of the gels. By adding different masses of nickel chloride, samples with different pore structures were obtained. The micropore volume increased from 0.21 $cm^3\,g^{-1}$ of BNC-7 to 0.34 $cm^3\,g^{-1}$ of BNC-9 and the mesopore volume increased by 0.1 $cm^3\,g^{-1}$. Large portions of mesopores and macropores formed when further increasing the mass of nickel chloride in the gels of BNC-9, 12 and 15. Cyclic voltammetric and galvanostatic charge/discharge were employed to investigate the electrochemical behavior of the materials. All of the BNC samples had near rectangular shape I–V curves with slightly distorted at a sweep rate of $2\,mV\,s^{-1}$, which is characteristic of electrochemical capacitor. The deviation from the imaginary rectangular may be due to the pseudocapacitive effects. The nitrogen, boron and oxygen incorporated into the carbon matrix enhanced the wettability between the electrolyte and electrode materials, and the introduction of heteroatoms may result in the pseudocapacitive effect. The values of capacitances per surface area of all the samples are larger than usually reported for the double-layer capacitance (0.1–0.2 $F\,m^{-2}$), which highlight the pseudocapacitive effect of boron and nitrogen co-doping. The charge/discharge curves of both BNC-9 and BNC-15 have near triangular shapes, reflecting their good capacitive performances. BNC-9 has the largest specific capacitance and the highest capacitance retention value was obtained in BNC-15. The specific capacitances are 268 and 173 $F\,g^{-1}$ with the current of $0.1\,A\,g^{-1}$ for BNC-9 and BNC-15, respectively. When the applied current was increased from 0.1 to $1\,A\,g^{-1}$, the capacitances remained 59% and 72% for BNC-9 and BNC-15, respectively. The power density of BNC-15 is larger than that of BNC-9, but BNC-9 possesses the larger energy density at the same constant current. When the current was set as $1\,A\,g^{-1}$, the energy densities and power densities for BNC-9 and BNC-15 were 3.8/3.0 $Wh\,kg^{-1}$ and 165/201 $W\,kg^{-1}$, respectively. Thus, BNC-15 may be more suitable to apply in high-power-demanded occasion, while BCN-9 tends to store more energy.

In summary, boron as well as nitrogen doping can enhance the specific capacitance because of pseudocapacitive effect. And samples with larger partial of mesopores have better high rate response, while highly microporous samples can store more charges. The results are helpful to understand the effect of heteroatoms doped into carbon matrix on the capacitive behaviors and design different types of supercapacitors applied in high-power-demanded or high-energy-demanded occasions in future.

Acknowledgements

This work was financially supported by Chinese National Science Foundation (No. U0734002), "Project of One Hundred Outstanding

Talents" of Chinese Academy of Sciences and Shanghai Nanotechnology Promotion Center (No. 0652nm025).

References

[1] T.A. Centeno, G. Lota, E. Frackowiak, F. Stoeckli, Electrochim. Acta 53 (2008) 2210–2216.
[2] E. Frackowiak, Phys. Chem. Chem. Phys. 9 (2007) 1774–1785.
[3] A.G. Pandolfo, A.F. Hollenkamp, J. Power Sources 157 (2006) 11–27.
[4] T. Hyeon, J. Lee, J. Kim, Adv. Mater. 18 (2006) 2073–2094.
[5] Z. Hu, M.P. Srinivasan, Y. Ni, Adv. Mater. 12 (2000) 62–65.
[6] W.P. Walawender, T. Zhang, L.T. Fan, M. Fan, D. Daugaard, R.C. Brown, Chem. Eng. J. 105 (2004) 53–59.
[7] A.C. Lua, T. Yang, J. Colloid Interf. Sci. 267 (2003) 408–417.
[8] Y. Gogotsi, J. Chmiola, G. Yushin, C. Portet, P. Simon, P.L. Taberna, Science 313 (2006) 1760–1763.
[9] M. Arulepp, J. Leis, M. Lätt, F. Miller, K. Rumma, E. Lust, A.F. Burke, J. Power Sources 162 (2006) 1460–1466.
[10] P. Simon, C. Largeot, C. Portet, J. Chmiola, P.-L. Taberna, Y. Gogotsi, J. Am. Chem. Soc. 130 (2008) 2730–2731.
[11] H. Cheng, D. Wang, F. Li, M. Liu, G. Lu, Angew. Chem. Int. Ed. 47 (2008) 373–376.
[12] F. Béguin, C.O. Ania, V. Khomenko, E. Raymundo-Piñero, J.B. Parra, Adv. Funct. Mater. 17 (2007) 1828–1836.
[13] D. Zhao, Z. Jiang, W. Li, D. Chen, Z. Li, Y. Shi, Y. Wan, G. Wang, Carbon 45 (2007) 1757–1763.
[14] J. Ozaki, N. Kimura, T. Anahara, A. Oya, Carbon 45 (2007) 1847–1853.
[15] M. Kawaguchi, T. Kawashima, J. Chem. Soc. Chem. Commun. 21 (1993) 1133–1134.
[16] S. Shiraishi, M. Kibe, T. Yokoyama, H. Kurihara, N. Patel, A. Oya, Y. Kaburagi, Y. Hishiyama, Appl. Phys. A 82 (2006) 585–591.
[17] T.C.M. Chung, Y. Jeong, Q. Chen, A. Kleinhammes, Y. Wu, J. Am. Chem. Soc. 130 (2008) 6668–6669.
[18] S. Mondal, A.K. Banthia, J. Eur. Ceram. Soc. 25 (2005) 287–291.
[19] A. Sinha, T. Mathata, B.P. Sharma, J. Nucl. Mater. 301 (2002) 165–169.
[20] T. Kyotani, K. Matsuoka, Y. Yamagishi, T. Yamazaki, N. Setoyama, A. Tomita, Carbon 43 (2005) 876–879.
[21] R. Mokaya, Z. Yang, Y. Xia, J. Am. Chem. Soc. 129 (2007) 1673–1679.
[22] T. Kyotani, T. Nagai, S. Inoue, A. Tomita, Chem. Mater. 9 (1997) 609–615.
[23] R. Trehan, Y. Lifshitz, J.W. Rabalais, J. Vac. Sci. Technol. A 8 (1990) 4026–4032.
[24] C. Guimon, D. Gonbeau, G. Pfister-Guillouzo, O. Dugne, A. Guette, R. Naslain, M. Lahaye, Surf. Interf. Anal. 16 (1990) 440–445.
[25] Y.M. Shul'ga, T.M. Moravskaya, S.V. Gurov, V.I. Chukalin, Y.G. Borod'ko, Poverkhnost 10 (1990) 155.
[26] A. Vinu, M. Terrones, D. Golberg, S. Hishita, K. Ariga, T. Mori, Chem. Mater. 17 (2005) 5887–5890.
[27] N. Sevinç, A. Aydoğdu, J. Eur. Ceram. Soc. 23 (2003) 3153–3161.
[28] J. Chen, F. Cheng, J. Liang, J. Zhao, Z. Tao, Chem. Mater. 20 (2008) 1889–1895.
[29] R. Mokaya, Z. Yang, Y. Xia, X. Sun, J. Phys. Chem. B 110 (2006) 18424–18431.
[30] R. Mokaya, A. Pacula, J. Phys. Chem. C 112 (2008) 2764–2769.
[31] T. Nakajima, M. Koh, Carbon 38 (2000) 1947–1954.
[32] D. Hulicova, M. Kodama, H. Hatori, Chem. Mater. 18 (2006) 2318–2326.
[33] J.M. Rojo, A.B. Fuertes, Fernando Pico, J. Power Sources 133 (2004) 329–336.
[34] Q. Xu, B. Liu, H. Shioyama, T. Akita, J. Am. Chem. Soc. 130 (2008) 5390–5391.
[35] P. Simon, C. Portet, P.L. Taberna, E. Flahaut, C. Laberty-Robert, Electrochim. Acta 50 (2005) 4174–4181.